Passive acoustic monitoring of bed load discharge in a large gravel bed river

Thomas Geay, P. Belleudy, Cedric Gervaise, H. Habersack, J. Aigner, A. Kreisler, H. Seitz, J. B. Laronne

HAL Id: hal-01660911

https://hal.univ-grenoble-alpes.fr/hal-01660911

Submitted on 13 Aug 2021

RESEARCH ARTICLE

Key Points:
- Hydrophone signals in a large gravel bed river are correlated to bed load discharge monitored by geophones
- The listening distance of a hydrophone is estimated at 5 to 10 m
- Passive acoustic signals recorded in a large gravel bed river are processed using short-term frequency representations

Supporting Information:
- Supporting Information S1

Correspondence to:
T. Geay,
th.geay@gmail.com

Passive acoustic monitoring of bed load discharge in a large gravel bed river

T. Geay[1,2] (iD), P. Belleudy[1] (iD), C. Gervaise[2], H. Habersack[3], J. Aigner[3], A. Kreisler[3], H. Seitz[3], and J. B. Laronne[1,4]

[1]Université Grenoble Alpes, CNRS, IRD, Grenoble INP, IGE, Grenoble, France, [2]Université Grenoble Alpes, Grenoble INP, CNRS, GIPSA-Lab, Grenoble, France, [3]Department of Water Management, Hydrology, and Hydraulic Engineering, University of Bodenkultur, Vienna, Austria, [4]Department of Geography and Environmental Development, Ben-Gurion University of the Negev, Beer Sheva, Israel

Abstract Surrogate technologies to monitor bed load discharge have been developed to supplement and ultimately take over traditional direct methods. Our research deals with passive acoustic monitoring of bed load flux using a hydrophone continuously deployed near a river bed. This passive acoustic technology senses any acoustic waves propagated in the river environment and particularly the sound due to interparticle collisions emitted during bed load movement. A data set has been acquired in the large Alpine gravel-bedded Drau River. Analysis of the short-term frequency response of acoustic signals allows us to determine the origin of recorded noises and to consider their frequency variations. Results are compared with ancillary field data of water depth and bed load transport inferred from the signals of a geophone array. Hydrophone and geophone signals are well correlated. Thanks to the large network of deployed geophones, analysis of the spatial resolution of hydrophone measurements shows that the sensor is sensitive to bed load motion not only locally but over distances of 5–10 m (10–20% of river width). Our results are promising in terms of the potential use of hydrophones for monitoring bed load transport in large gravel bed rivers: acoustic signals represent a large river bed area, rather than being local; hydrophones can be installed in large floods; they can be deployed at a low cost and provide continuous monitoring at high temporal resolution.

1. Bed Load Monitoring

1.1. Introduction

Bed load transport is a fundamental process in alluvial rivers, with implications for channel morphology, sediment budgets, contaminant transport, aquatic habitat, and human infrastructure along river corridors. Pressure-difference bed load samplers are widely used to determine bed load flux. One such device is the Helley-Smith sampler [*Helley and Smith*, 1971; *Emmett*, 1980], with modern derivates such as the Toutle River bed load sampler [*Childers*, 1999]. However, problems related to spatial and temporal variability of bed load measurements using such samplers have been documented [*Gomez et al.*, 1989; *Vericat et al.*, 2006]. Additionally, physical sampling is time consuming, expensive, at times dangerous, and often inappropriate for large gravel bed rivers [*Camenen et al.*, 2012], especially during large floods.

Hence, the scientific community became interested in surrogate bed load technologies predominantly using active and passive acoustics. *Mühlhofer* [1933] was the first to propose a system using passive acoustics to monitor bed load motion. Despite large advances in the use of bed load-surrogate technologies, none of them are currently accepted for operational use [*Gray et al.*, 2010]. Our study investigates the potential of passive acoustics to monitor bed load transport in a gravel-bedded river. In the following subsections, we address the use of surrogate methods for measuring bed load discharge in such environments.

1.2. Surrogate Monitoring of Bed Load Discharge in Large Gravel Bed Rivers

Several surrogate techniques have been developed for monitoring bed load discharge. The largest number of deployed sensors and most published are those based on the acoustic monitoring of gravel impacts on steel plates [*Rickenmann and McArdell*, 2007; *Krein et al.*, 2008; *Tsakiris et al.*, 2014; *Barrière et al.*, 2015a; *Hilldale et al.*, 2015; *Wyss et al.*, 2016] or pipes [*Mizuyama et al.*, 2010] fixed onto the river bed. This type of monitoring technique has almost exclusively been deployed in mountain streams [*Rickenmann et al.*,

2012, 2014]. They function well in small, shallow stable river reaches such as on check dams or Sabo dams as termed in Japan. The system has the advantage of requiring little maintenance. Successful calibrations have been undertaken for several orders of magnitude of bed load flux [*Rickenmann et al.*, 2012], and the method has been shown to be robust [*Rickenmann et al.*, 2014]. The main disadvantages of this technique are the requirement for a stable section and the relatively expensive cost of civil engineering works for installation and maintenance.

Acoustic Doppler current profilers (ADCPs) are nowadays operationally used to measure flow velocities and to determine water discharge; they have also been employed to monitor suspended sediment concentration [*Topping et al.*, 2007; *Thorne et al.*, 2011; *Moore et al.*, 2012]. Recently, ADCPs have been successfully used to monitor bed load transport in large gravel bed rivers [*Rennie et al.*, 2002; *Rennie and Church*, 2010; *Lorang and Tonolla*, 2014]. An ADCP may be used as a continuous monitoring device at a given location, but it is, therefore, local, does not represent the entire cross section, and commonly does not remain on site. The use of an ADCP requires presence at the site and is difficult to use in floods, where floating wood debris and surface waves may endanger the instrument. Indeed, ADCPs are commonly not deployed under severe flow conditions. Another indirect acoustic method has recently been proposed [*Muste et al.*, 2016] using a multibeam technology to map the bathymetry. It allows calculation of bed load discharge in large rivers but is very labor intensive and requires movement of bed forms (bars). As with ADCPs, the above approach is not easily used during floods.

New monitoring techniques are required for large gravel bed rivers to enable operation under a variety of normal and extreme hydrologic and hydraulic conditions, especially during flood events as well as for continuous-automatic data acquisition. Regarding these operational aspects, sensors that are easy to deploy are of primary interest for the development of sediment observatories. The use of seismic arrays may be a satisfying alternative for monitoring bed load transport in steep channels [*Hsu et al.*, 2011; *Burtin et al.*, 2011; *Tsai et al.*, 2012; *Schmandt et al.*, 2013; *Burtin et al.*, 2014; *Díaz et al.*, 2014; *Gimbert et al.*, 2014; *Roth et al.*, 2014, 2016]. They have the advantage of being noninvasive as the sensor is located outside of the river. The application of seismic methods is constrained by the occurrence of other seismic noises—physical processes such as turbulence [*Gimbert et al.*, 2014], rain events [*Roth et al.*, 2016], and anthropogenic noise such as road traffic [*Barrière et al.*, 2015b]. A recent study has shown that seismic methods could also be applicable to low-gradient gravel bed rivers [*Barrière et al.*, 2015b].

Another alternative technique was introduced by *Bedeus and Ivicsics* [1964]. It is based on recording bed load self-generated noise. A hydrophone is used to sense acoustic waves resulting from intercollisions of sedimentary particles moving on the bed. The deployment of a hydrophone is as simple as the deployment of turbidity meters or water level sensors, widely used in fluvial monitoring. Like seismic methods, hydrophones may record a variety of noises, particularly those originating from hydrodynamic processes, making it challenging to isolate acoustic signals arising from bed load transport. Our study deals with the calibration of passive acoustic measurement to estimate bed load flux and grain-size distribution. An overview of the existing literature on passive-acoustic studies is presented below.

1.3. Self-Generated Noise in Laboratory Experiments

While standing near a river actively transporting bed load, one can hear particle collisions. It appears that the human ear is able to sense acoustic waves in a maximum range of 20–20,000 Hz [*Rossing et al.*, 2001] and, therefore, to recognize the sound generated by interparticle collisions in this frequency band. However, an objective analysis using signal processing methods is more complex. Several laboratory experiments have demonstrated that the root-mean-square value of the acoustic pressure (p_{rms}, Pa) is correlated with bed load flux. p_{rms} has been related to the mass of bed load transport (M) with power laws [*Johnson and Muir*, 1969; *Thorne*, 1985, 1986; *Rouse*, 1994; *Voulgaris et al.*, 1995]:

$$p_{rms} = \beta M^{\gamma}, \tag{1}$$

where β and γ are empirical parameters dependent on the monitoring system and on sediment characteristics. The parameter γ is dependent on the grain-size distribution of the moving bed load mixture [*Thorne*, 1986]. The acoustic frequency spectrum is mainly altered by sediment characteristics including size, shape, and mineralogy [*Thorne and Foden*, 1988; *Thorne*, 2014]. These studies show that particle velocity affects the generated amplitudes but much less so the frequency content of the signal. The central frequency of

the signal decreases as particle size increases, just as in string instruments the tone frequency decreases from a narrow string to a broader string. Similar observations have been made using impact plate systems [*Møen et al.*, 2010; *Barrière et al.*, 2015a]. Empirical laws have been proposed to link frequency parameters to bed load particle sizes [*Thorne*, 1985, 1986, 2014]. For uniform grain-size distributions,

$$f_{peak} = \frac{224}{D^{0.9}}$$

(2)

$$fc = \frac{209}{D^{0.88}},$$

(3)

where D is the grain diameter (m), f_{peak} is the frequency corresponding to the maximum of the power spectral density (PSD), and fc is the central frequency of the PSD, which satisfies the following equality [*Thorne*, 1986]

$$\int_{fmin}^{fc} PSD(f)df = \int_{fc}^{fmax} PSD(f)df,$$

(4)

where the significant region $[f_{min}, f_{max}]$ is given by $PSD(f) > 0.1 PSD_{max}(f)$.

1.4. Field Experiments With Hydrophones

Passive acoustic monitoring cannot be understood without considering soundscapes [*Pijanowski et al.*, 2011]. A soundscape comprises a variety of sounds originating from geophysical activity (rain, wind, rock falls, and snow avalanches), wild life (birds, marine mammals, and fish), or human activities (traffic and engines). Pressure fluctuations sensed by a hydrophone contain a mix of these sounds that propagate in the monitored environment. River soundscapes have been shown to be correlated to hydrogeomorphological characteristics [*Tonolla et al.*, 2009, 2010, 2011; *Wysocki et al.*, 2007]. For example, hydrodynamic noises are generated by surface waves or pressure fluctuations induced by turbulence [*Tonolla et al.*, 2009]. In large rivers, human activities such as boat traffic are also suspected of impacting the acoustic signals [*Vračar and Mijić*, 2011].

Pressure fluctuations induced by turbulence originate from the inherent turbulent character of natural flows and overall from the presence of an object (the hydrophone) in the flow [*Wenz*, 1962; *Strasberg*, 1979; *McEachern and Lauchle*, 1995; *Lauchle et al.*, 2002]. Considered as a pseudonoise (because it does not propagate), these pressure fluctuations create noise in the low-frequency range (<100 Hz) and the power spectral slope of turbulent noise has been observed to decrease by 1 to 3 orders of magnitude per decade [*Wenz*, 1962; *Strasberg*, 1979; *Lauchle et al.*, 2002, *Barclay and Buckingham*, 2013].

Noise of surface waves dominates in the midfrequency range of 500–2000 Hz [*Lugli and Fine*, 2003; *Tonolla et al.*, 2009, 2010]. It can mask part of the noise generated by moving pebbles ($D \sim 10$ cm). This sound is generated by the breaking of surface waves, producing noisy bubble plumes, which can be compared to surf noise in marine environments [*Wenz*, 1962; *Loewen and Melville*, 1991; *Deane*, 1997, 2000]. In rivers, the intensity of breaking waves is related to the ratio between water depth and river bed roughness [*Tonolla et al.*, 2009]. This is the reason that we consider that the use of a hydrophone is more relevant to large gravel bed rivers where water depth is sufficiently large so that the intensity of breaking waves is low.

Hydrophones have been deployed for bed load monitoring in natural streams [*Johnson and Muir*, 1969; *Jonys*, 1976; *Barton et al.*, 2010; *Lorang and Tonolla*, 2014; *Marineau et al.*, 2015]. Some experiments have been constrained by the occurrence of other sources of noise in the river [*Johnson and Muir*, 1969; *Jonys*, 1976]. Because of the difficulty in measuring different processes that produce noise in a river, such as sediment transport or flowing water (i.e., turbulence or surface waves), observations in prior studies were generally limited to comparing time variations of acoustic energy and water discharge. Hysteresis effects have been observed between root-mean-square acoustic pressure and water discharge [*Barton et al.*, 2010]. Similar observations were made in some of the seismic studies [*Hsu et al.*, 2011; *Tsai et al.*, 2012; *Schmandt et al.*, 2013; *Díaz et al.*, 2014; *Roth et al.*, 2014]. These observations suggest that the recorded sound was not generated by a variable dependent on discharge alone, such as entrained-bubble collapse or turbulence. This issue is important because some hysteretic responses have been argued to include not merely bed load transport but also flow-induced turbulent noise [*Gimbert et al.*, 2014]. Finally, none of the prior studies were able to set up in field experiments a robust relationship between acoustic signals of the river soundscape and bed load flux.

1.5. Objectives

The main focus of this study is to determine the extent to which bed load sounds recorded in a large gravel bed river are related to bed load flux and texture (i.e., size of transported material). A recurrent deficiency in prior experiments with hydrophones is the accuracy of the direct, comparative techniques used to monitor bed load flux. Pressure-difference bed load samplers have generally been used although their reliability is questionable in gravel bed rivers [*Vericat et al.*, 2006]. Observations were also limited by the use of fairly simple processing methods, restricting interpretation of the acoustic signals. Signals have hitherto been processed by simply computing their root-mean-square pressure in specific frequency bands [*Johnson and Muir*, 1969; *Jonys*, 1976; *Barton et al.*, 2010; *Lorang and Tonolla*, 2014; *Marineau et al.*, 2015]. Our study is, therefore, structured around two main points: (1) the use of signal processing tools to examine the structure of the short-term frequency response of a hydrophone. Origins of recorded noises are discussed, and estimation of typical characteristics of bed load self-generated noise is computed; and (2) the hydrophone response is then analyzed based on data derived during several weeks of continuous monitoring. The evolution of the frequency content is discussed using bed load slot sampler measurements at this study site. Root-mean-square acoustic pressures are compared to high-quality bed load measurements made by a large network of geophones [*Habersack et al.*, 2016]. This network is distributed across the entire cross section and enables the investigation of spatial properties of hydrophone measurements.

2. Methods

2.1. Study Area

The Drau River, a Danube River tributary, is a large gravel bed river governed by a nivo-glacial flow regime. The monitoring section is located at Dellach/Drau in Carinthia (Austria), draining a basin of 2112 km². Respective minimum and maximum water discharges of 13.7 and 325 m³ s⁻¹ have been observed since 2004, with a mean annual discharge of 69.2 m³ s⁻¹. The studied area is a straight river reach with a 0.19% longitudinal bed slope, having a slightly asymmetric 50 m wide cross section, a measured subsurface median diameter D_{50} of 38.7 mm and a measured surface median diameter of about 65 mm. With respect to sediment transport, the Drau River is one of the most instrumented European rivers. Water level is monitored with an Ott Kempten Inc. (Nimbus) pressure sensor. Bed load monitoring is achieved not merely by Helley-Smith sampling [*Habersack and Laronne*, 2002; *Habersack et al.*, 2008], but the section also includes direct and surrogate bed load monitoring methods with three automatic slot samplers and 40 geophones [*Habersack et al.*, 2010] (Figure 1). The monitored water level is the water depth above geophones G#9 to G#40.

2.2. Geophone Monitoring

Indirect bed load sensors were installed in 2006 to increase the spatial and temporal resolution of bed load monitoring. This surrogate bed load monitoring technology comprises geophone sensors mounted on steel plates embedded in the river. Plate vibrations are recorded when moving gravel particles impact a geophone sensor. These are processed to obtain the number of detected pulses (IMP) and the square integral of the signal (IQA), both of which have been shown to be correlated with bed load discharge in Swiss and Austrian mountain streams [*Rickenmann and McArdell*, 2007; *Rickenmann and Fritschi*, 2010; *Turowski et al.*, 2011; *Habersack et al.*, 2012; *Rickenmann et al.*, 2014]. For the first time in a large gravel bed river, the Drau has been instrumented with a large number of geophones to continuously monitor its cross sectional and total bed load discharge [*Habersack et al.*, 2010]. The number of impulses recorded by a geophone has been shown to be linearly correlated to the bed load mass (*M*) of larger (approximately *D* > 20 mm) sedimentary particles [*Rickenmann et al.*, 2012, 2014]:

$$\text{IMP} = k_b M, \tag{5}$$

where k_b is a site-specific empirical coefficient. Similarly, the square integral of geophone signals has been shown to be correlated with bed load mass using power law relationships [*Møen et al.*, 2010; *Rickenmann et al.*, 2014]:

$$\text{IQA} = k M^{\alpha}, \tag{6}$$

where *k* and *α* are empirical coefficients. As with hydrophones, the geophone calibration parameters k_b, *k*, and *α* of equations (5) and (6) are influenced by particle size [*Rickenmann et al.*, 2014].
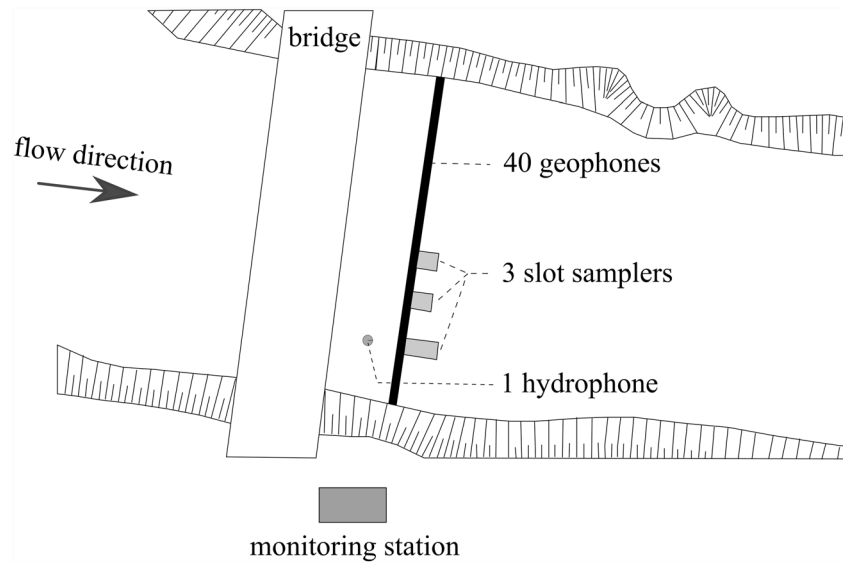
Figure 1. Schematic plan view of the monitoring station at Dellach im Drautal (Austria). The reach is 50 m wide; 40 geophone plates are distributed along the entire cross section. Geophones G#1 and G#40 are located near the left and right banks, respectively. Three slot samplers are located downstream of the geophone section, the liftable right-bank sampler immediately downstream of geophone G#32, upstream of which we located the hydrophone.

In this study, we use both the square integrals of the signal (IQA) and impulse counts (IMP). Using the square integral provides better resolution than counts of discrete impulses because IQA is a continuous measure of energy. However, care has to be taken in using the square integral of the signal, because it may be affected and even dominated by electronic and seismic noises. An increasing contribution of ambient noise is expected for decreasing (small) values of bed load flux. In such cases, additional analyses are needed for proper interpretation of the IQA data (e.g., by using spectral characteristics of the signal or comparative bed load measurements to separate the bed load transport signal from ambient noise). As raw signals of the geophones are not recorded, we cannot properly interpret IQA values to separate bed load noise from ambient noise. Our study will therefore mainly focus on the impulse count (IMP).

For our analysis, each geophone is considered to be representative of the average cross-sectional length between neighboring geophones l_i:

$$l_i = \frac{X_{i+1} - X_{i-1}}{2}, \tag{7}$$

where X_i is the cross-sectional location of the center of a given geophone plate, with geophones nonuniformly distributed over the cross section. The total river bed load activity is considered using a weighted mean of each geophone response over a specified period of time:

$$\overline{IMP} = \frac{1}{l} \sum_{i=1}^{40} l_i \cdot IMP_i \tag{8}$$

$$\overline{IQA} = \frac{1}{l} \sum_{i=1}^{40} l_i \cdot IQA_i, \tag{9}$$

where i refers to each geophone, IMP_i is the number of impulses normalized by the width of the geophone plate and the recording period (imp m^{-1} min^{-1}), IQA_i is the square integral of the signal normalized by the width of the geophone plate and the recording period (V^2 m^{-1} min^{-1}), and l is the entire width of the river.

Bed load transport is physically sampled by three large Reid-type slot samplers [*Reid et al.*, 1980]. The slot samplers are located downstream of the geophone plates in order to calibrate and to study the geophone system [*Habersack et al.*, 2010]. No hydrophone sampler calibration was undertaken during the deployment of the hydrophone in the Drau. A direct comparison between hydrophone and slot sampler measurements is, therefore, unavailable. However, geophone measurements were obtained during the
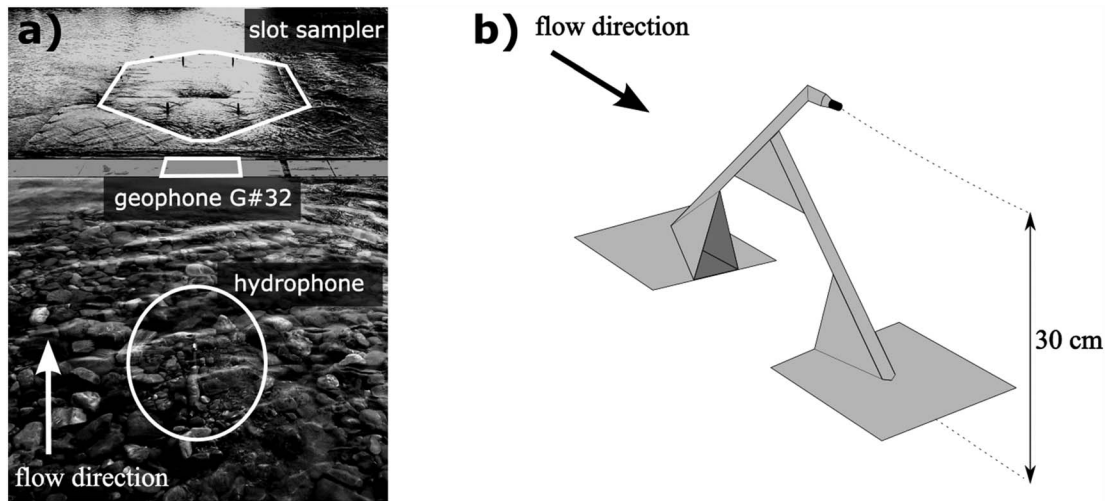
Figure 2. (a) Photo of the bed area showing the lining up of the hydrophone, geophone G#32, and the liftable Reid type slot sampler. (b) Scheme of the deployed hydrophone. It is mounted on a 32 mm stainless steel tube, and it is reinforced by foot plates. The base of the structure is located below the river bed level, under approximately 10 cm of gravel. The structure is fixed to a concrete base made in the river bed.

hydrophone deployment and are used to estimate bed load transport rates. Several hours of continuous monitoring of bed load flux in one Reid slot sampler and synchronous monitoring by nearby plate geophones [*Habersack et al.*, 2016] show high correlations between geophone data (IMP_i, IQA_i) and specific bed load transport rates (for $D > 22.4$ mm):

$$IMP_i = 3.54 \cdot q_{si} \qquad (r^2 = 0.99) \tag{10}$$

$$IQA_i = 0.0004 \cdot q_{si}^{0.84} \qquad (r^2 = 0.96), \tag{11}$$

where q_{si} is the specific bed load discharge in $kg\,m^{-1}\,min^{-1}$. IMP, IQA, and q_s are mean values per hour. We relate hydrophone measurements to recorded $\overline{IMP}$ and $\overline{IQA}$ values, from which bed load transport rates are inferred, as discussed in section 3.2.

2.3. Acoustic Monitoring

Sound was acquired using a Bruël and Kjaer-type 8103 calibrated hydrophone with a sensitivity of -219.7 dB re 1 V/μPa (i.e., in reference to 1 V/μPa) and a flat frequency response in the range 0.1–100 kHz (±3 dB). The hydrophone was connected to a conditioning preamplifier (45.6 dB gain and 100 kHz cutoff frequency Chebyshev filter) via a 70 m cable. Data were digitized using National Instrument devices (CRio-9014 with a 9201 module). Acoustic data were sampled at a rate of 500 kHz with 12 bit resolution and stored on an external hard disk. The acoustic monitoring system was slaved to the water level monitoring system. For water depths lower than 1 m, sound was recorded for a duration of 1 min every 30 min and every 10 min when water depth exceeded 1 m. The hydrophone was installed upstream and in line with geophone G#32 and with the liftable Reid-type slot sampler (Figure 2a). The hydrophone was located about 20 cm above the river bed, facing downstream to avoid direct impacts on the sensor (Figure 2b). It was mounted on a stainless steel structure fixed on a concrete foundation in the river bed. Hydrophone signals are expressed in terms of pressure fluctuations (see supporting information Text S1).

2.4. Processing of the Acoustic Data Set

The aim of this part is to analyze the short-term response of the hydrophone signals (at a minute time scale). Time-frequency representations of the acoustic signals are shown and discussed to describe the different origins of the recorded noise. Estimation of the power spectral density (PSD) is then discussed, and an algorithm is proposed to process the acoustic data set.

2.4.1. Short-Term Response of the Hydrophone

A time-frequency analysis, coupled with careful listening, has been used to interpret the hydrophone signals. A short-term Fourier transform algorithm has been applied for each recording of 1 min duration. Two
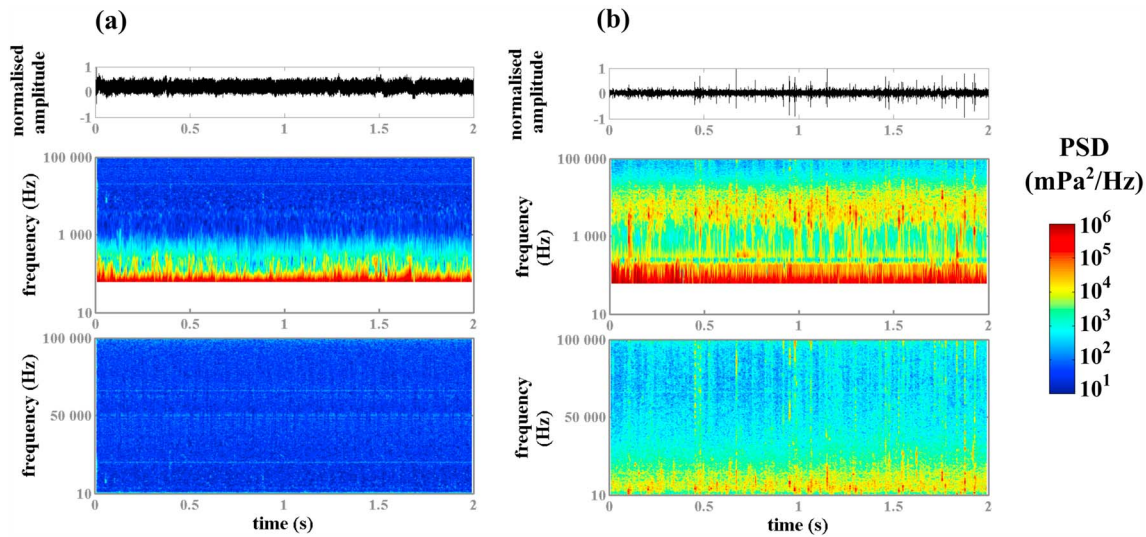
Figure 3. Temporal waveforms, semilogarithmic spectrograms, and linear spectrograms of acoustic signals in the Drau River: (a) on 18 March 2012 at low flow and (b) on 1 August 2012 at intermediate flow.

spectrograms of characteristic recordings are shown in Figure 3. Signals have also been analyzed by their spectral probability density (SPD) using the *Merchant et al.* [2013] algorithm (Figure 4). The SPD presents the full range of power spectral density (PSD) observed during a certain period of time. In Figure 4, we present statistical spectra (or percentiles) resulting from the SPD. In this study, 1 min signals have been segmented using Hanning windows of 0.05 s and a recovery rate of 66%.

The first signal was recorded on 18 March 2012 at low flow conditions (Figures 3a and 4a). At this stage no bed load movement was expected. Below 1000 Hz the noise sounds like the sensation of wind around ears. Its power randomly fluctuates in a band of 2 orders of magnitude and its spectral slope decreases about 2 orders of magnitude (Figure 4a). These spectral characteristics are typical of turbulence around the hydrophone (see section 1.4). Above 1000 Hz, the signal is composed of residual electronic noises, showing the limitation of our monitoring system. The acoustic signal recorded on 18 March 2012 is fully dominated by turbulence-induced noise and electronic noises. The second signal was recorded on 1 August 2012 during the snow melt season. On this date bed load activity was recorded by the geophone array. As observed in Figure 3a, the effect of turbulence around the hydrophone is still present at low frequency, below 300 Hz (Figure 4b). The main difference between Figures 3a and 3b is observed above 300 Hz. Some short impulses can be clearly heard. They sound like the crackling of flames. They are well represented by vertical lines in the
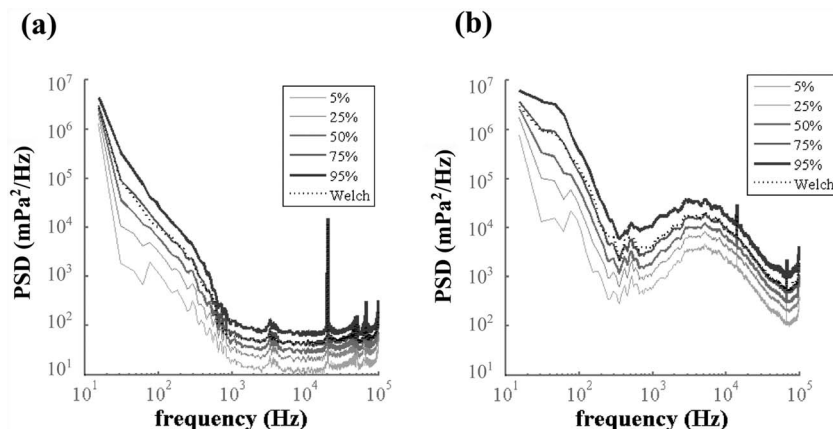

Figure 4. Power spectral density (PSD) estimates computed using the *Welch* [1967] and statistical methods [*Merchant et al.*, 2013]: (a) on 18 March 2012 at low flow and (b) on 1 August 2012 at intermediate flow.

linear spectrogram (Figure 3b). These impulses generate wideband signals dominating the signal above 300 Hz (Figure 4b). The power maximum of these impulses is located around 4000 Hz. Equation (2) predicts a particle diameter of 41 mm, close to the subsurface median diameter D_{50} of 38.7 mm at the study site. Due to their observed temporal waveform, the impulse durations are on the order of a millisecond, close to the duration predicted by *Thorne*'s [1988] model. According to these characteristics, we can assume that these impulses are the result of bed load self-generated noise, made by impacts between bed load particles. Statistical spectra indicate that the content of the signal is stable over the recorded minute; the 5th percentile exhibits the same shape as the 95th percentile (Figure 4b). The signal power fluctuates in a band of 2 orders of magnitude, but the shapes of spectra do not change between percentiles. The signal is, indeed, made of a continuum of impulses. The closest impacts generate detectable impulses in the signal, while numerous distant impulses generate a background colored noise, where individual impulses are not clearly detectable.

2.4.2. Acoustic Parameters

To summarize the information contained in the monitored acoustic waves, each signal has been represented by its median power spectral density (PSD). The method is based on segmenting signals of 1 min duration in short segments of 0.05 s. The median power was computed in each frequency bin of the spectrogram (see supporting information Text S2). In this study, Hanning windows of 0.05 s with 50% overlap were used. The "median PSD" was preferred to the Welch method, as this enabled filtering of extreme events such as direct impingement of gravel on the hydrophone structure. For simplicity, the median PSD is noted PSD in the following. The acoustic signal is also considered by its root-mean-square pressure (p_{rms}), representing the power of the signal in a given frequency band:

$$p_{rms} = 2 \int_{f_{min}}^{f_{max}} PSD(f) df, \tag{12}$$

where f_{min} and f_{max} are the limits of a chosen frequency band. As justified hereafter in section 3.1, root-mean-square acoustic pressures have been computed in two frequency bands: p_{rms} computed (1) over the 1000–60,000 Hz frequency band is denoted by $p_{rms,b}$ (*b* for bed load generated noise) and (2) over the 10–100 Hz frequency band is denoted by $p_{rms,t}$ (*t* for turbulence-induced noise).

3. Results

The database covers a variety of hydrologic conditions for water depth in the range 70 to 190 cm, corresponding to typical water conditions at this time of year. The temporal variation of PSD, water depth, and weighted mean impulse rate ($\overline{IMP}$) are presented in Figure 5. The data set is presented in two periods during spring (period A) and summer floods (period B) followed by a period of 10 days without floods (period C). Overall, they represent about 76 h of raw acoustic data. Periods A and B contain several floods, reaching a maximum of water depth and impulse counts on 5 August 2012. Period C is representative of sunny summer days with daily variation of water discharge resulting from glacier melt.

3.1. Frequency Variations and Estimation of Mobile Grain Size

The acoustic data set has been classified into groups related to six levels of water depth (Figure 6a). The median of the PSD was computed for each group. Each PSD contains a local minimum located in the 100–1000 Hz frequency band. Below the frequency of the local minimum, the power decreases with increase in frequency at a rate of 2 orders of magnitude per decade. As described in section 1.4, this spectral slope is typical of turbulent processes. Above the frequency of the local minimum, the signal is fully dominated by bed load noise as suggested in section 2.4.1. Three frequency bands are identified: (1) the 10–100 Hz band, representative of turbulent processes; (2) the 1000–60,000 Hz band, representative of bed load noise; and (3) the middle frequency band 100–1000 Hz, dominant physical processes are turbulence at low flow and bed load noise at highest flow. The signature of bed load transport above 1000 Hz is always present during the study period. The dynamic range of this frequency band is much higher than the dynamic range of the lower frequency band (2 orders of magnitude compared to less than 1 order of magnitude). As water level increases, the central frequency of bed load PSD is observed to shift toward lower frequencies (Figure 6a). This observation can be explained by changes in bed load grain-size distribution: as shear stress increases larger pebbles are set in motion.
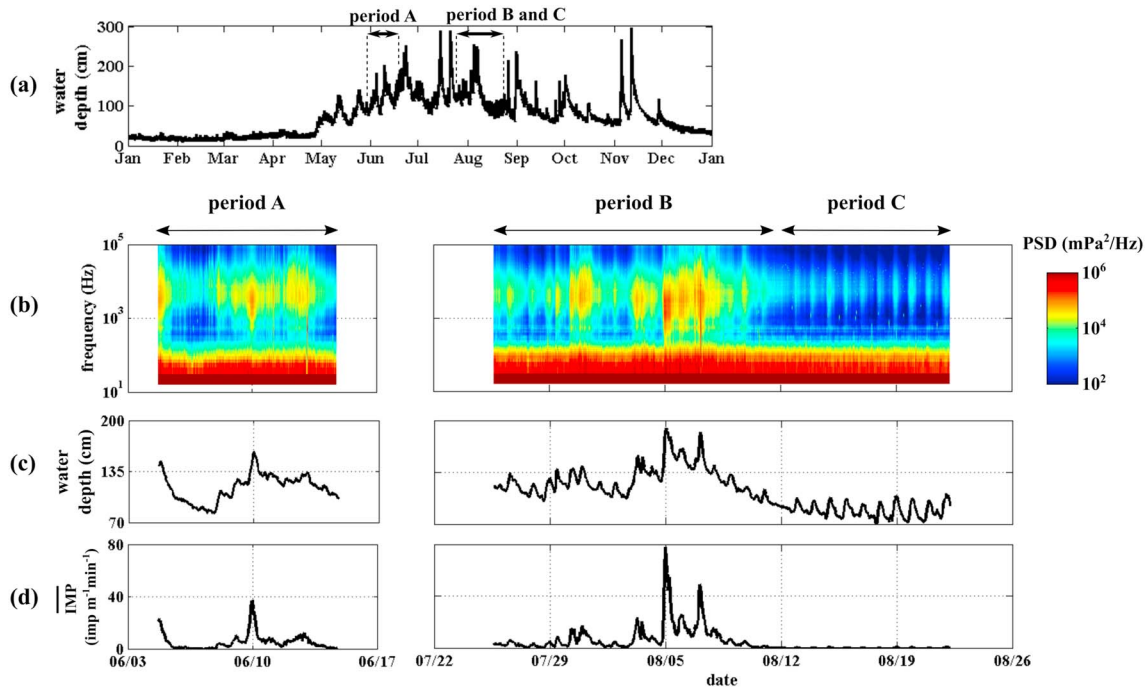
Figure 5. (a) Annual hydrograph and temporal variation of (b) power spectral density in mPa^2/Hz, (c) water depth in centimeters and (d) impulse rate recorded by the geophone array.

A characteristic grain size can be computed from the measured sound (Figure 6b) using the empirical equations (2) and (3). The effect of impact velocities on generated frequencies is here neglected. Diameters estimated with f_{peak} and equation (2) increase from 30 mm to 90 mm. Diameters computed with f_c and equation (3) are smaller, estimated between 10 mm to 25 mm. f_c was computed using equation (4) and excluding turbulence-induced noise (~10–100 Hz band). Typical diameters measured from the bed load slot sampler are also reported in Figure 6b. The D_{50} of Drau River bed load varies between 18 and 23 mm; this is similar to the bed load diameters estimated with the central frequency of the acoustic signals (f_c). The D_{90} was found to vary between 46 and 105 mm; this is close to the diameter estimated with the frequency peak (f_{peak}).

3.2. Does Hydrophone Output Represent Bed Load Flux?

The question addressed in this section deals with the use of root-mean-square pressure (p_{rms}) to estimate mean bed load flux. Hydrophone parameters (p_{rms}), geophone parameters ($\overline{IMP}, \overline{IQA}$), and water depth have been hourly averaged to deal with the difference in temporal resolution of measurements: geophone response is continuous, whereas hydrophone response is discrete. Combining equations (1), (5), and (6), the relationship between hydrophone (p_{rms}) and geophone parameters ($\overline{IMP}, \overline{IQA}$) has the following form:
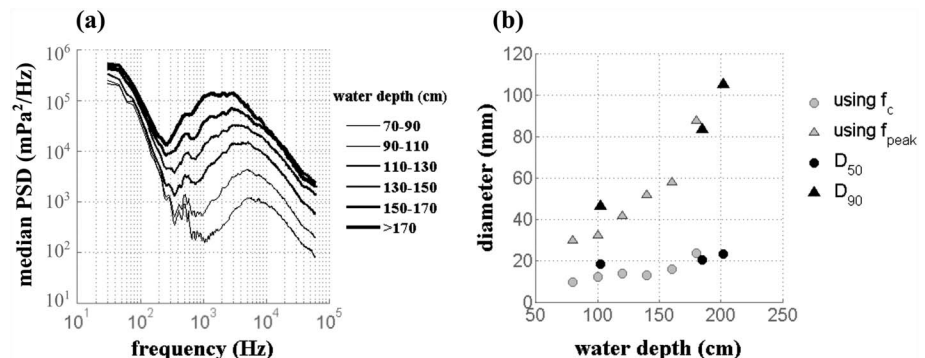

Figure 6. (a) Median power spectral density (PSD) for different water depths during all periods and (b) comparison of bed load grain sizes captured by the slot sampler with those predicted from equations (2) and (3) as a function of flow depth.

Table 1. Spearman Correlation Coefficient (r^2) for $\overline{\text{IMP}} \geq 1$
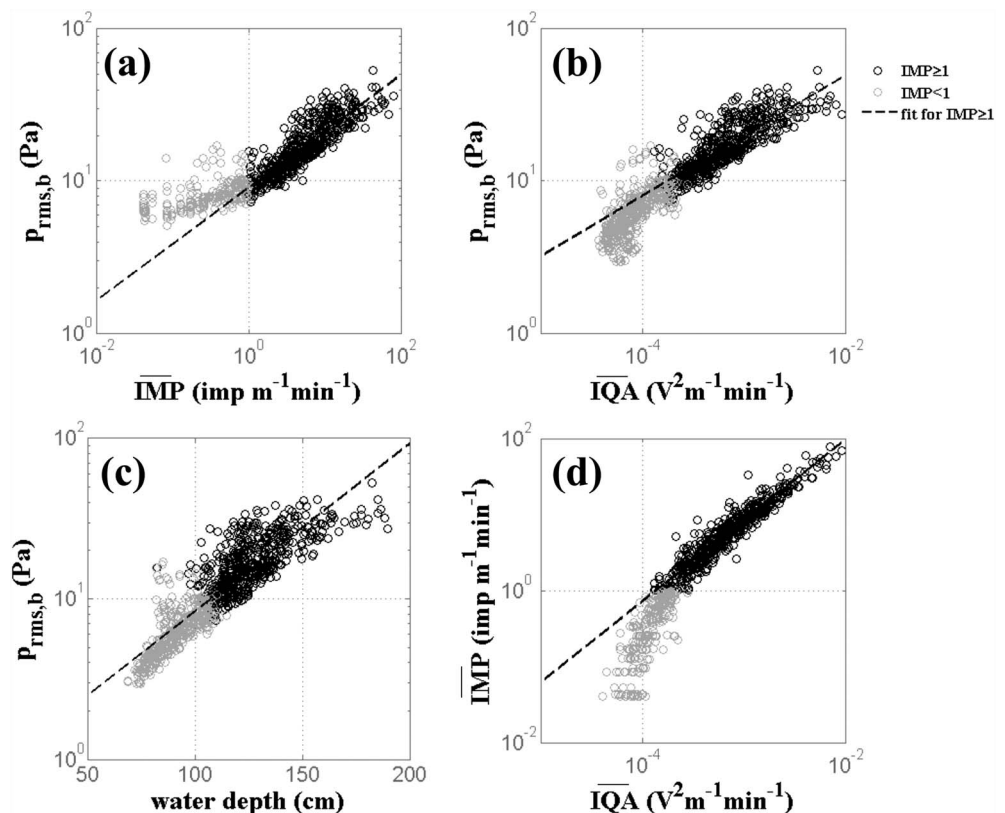
	$p_{\text{rms},b}$ (1–60 kHz)	$p_{\text{rms},t}$ (10–100 Hz)	$\overline{\text{IMP}}$	$\overline{\text{IQA}}$	Water Depth
$p_{\text{rms},b}$ (1–60 kHz)	-	0.39	0.85	0.81	0.64
$p_{\text{rms},t}$ (10–100 Hz)	-	-	0.42	0.42	0.38
$\overline{\text{IMP}}$	-	-	-	0.94	0.86
$\overline{\text{IQA}}$	-	-	-	-	0.88
Water depth	-	-	-	-	-

$$p_{\text{rms}} = A\overline{\text{IMP}}^{B} \tag{13}$$

$$p_{\text{rms}} = A'\overline{\text{IQA}}^{B'}, \tag{14}$$

where A, B, A′, and B′ are empirical parameters. Table 1 shows Spearman correlation coefficients between hydrophone ($p_{\text{rms},b}$, $p_{\text{rms},t}$), geophones ($\overline{\text{IQA}}$, $\overline{\text{IMP}}$), and water depth. Subscripts b and t refer to bed load transport and turbulence-induced acoustic pressures, respectively. $p_{\text{rms},b}$ is well correlated with $\overline{\text{IMP}}$ ($r^2 = 0.85$) and $\overline{\text{IQA}}$ ($r^2 = 0.81$) which, in turn, suggests that $p_{\text{rms},b}$ is well correlated with bed load flux. From equations (8) and (10), $\overline{\text{IMP}}$ is indeed shown to be linearly dependent on the total bed load flux transported in the Drau River.

Figure 7a shows the relationship between $p_{\text{rms},b}$ and $\overline{\text{IMP}}$. Two trends are considered: lower and higher bed load fluxes, the boundary between them set to $\overline{\text{IMP}} = 1$, which corresponds to a mean response of one impulse per minute per geophone. A change in the relationship between $\overline{\text{IMP}}$ and $\overline{\text{IQA}}$ is also observed at $\overline{\text{IMP}} \sim 1$ (Figure 7d). At low bed load fluxes, the number of observed impulses is lower than the count of impulses predicted by the fit for $\overline{\text{IMP}} \geq 1$ (Figures 7a and 7d). An impulse count occurs when a geophone signal reaches a threshold amplitude [*Rickenmann et al.*, 2014], i.e., when the particle impact is sufficiently "loud". Below this threshold, signals generated by bed load impacts can be sensed by the geophone in terms

Figure 7. (a) $p_{\text{rms},b}$ versus $\overline{\text{IMP}}$; (b) $p_{\text{rms},b}$ versus $\overline{\text{IQA}}$; (c) $p_{\text{rms},b}$ versus water depth; and (d) $\overline{\text{IMP}}$ versus $\overline{\text{IQA}}$.
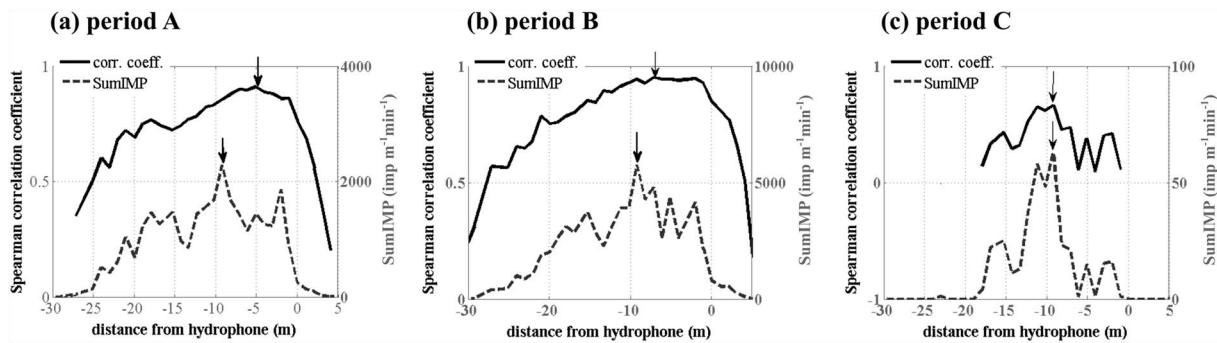
Figure 8. (a–c) Correlation coefficients (r^2) between geophone and hydrophone signals as a function of distance from the hydrophone during different measurement periods. Solid curve is the Spearman correlation coefficient (r^2) for relations between geophone activity (SumIMP) and hydrophone signal ($p_{rms,b}$, 1–60 kHz). The spatial variation of geophone activity (SumIMP) during each period is also shown (dashed curves). Arrows indicate the maxima of correlation and of geophone activity.

of $\overline{IQA}$ values but are insufficiently powerful to reach the amplitude triggering the impulse count (IMP = 0). This observation is discussed later (see section 4.2) and is interpreted as a limitation of the impulse count method to detect bed load motion for $D < 20$ mm. $\overline{IQA}$ reached a minimum value below 10^{-4} V^2 m^{-1} min^{-1} for $p_{rms,b}$ ranging from 3 to 7 Pa (Figure 7b). Unlike $\overline{IMP}$, $\overline{IQA}$ can detect small bed load impacts, but the signal energy has to be larger than the ambient noise (e.g., electronic and seismic noise generated by stresses on the bed) [*Gimbert et al.*, 2014]. Hence, the ambient noise sets the minimum value of $\overline{IQA}$ that can be detected. The relationship between $p_{rms,b}$ and water depth (Figure 7c) does not exhibit such changes at low flow. As explained in the previous section, the acoustic signal is fully dominated by impulses in the 1000–60,000 Hz frequency band. The hydrophone is, therefore, still representative of bed load motion for the lowest observed water discharge. Using the calibration curve of the geophone (10) and the fit for $\overline{IMP}$ > 1 (Figure 7) leads to the following relationship between p_{rms} and Q_s:

$$p_{rms,b} = 15Q_s^{0.37}, \tag{15}$$

where $p_{rms,b}$ is the root-mean-square of the acoustic pressure (Pa) in the 1000–60,000 Hz band and Qs is the total bed load flux (kg/min).

3.3. Spatial Resolution of Hydrophone Measurements

Geophone signals were often more variable than concomitant hydrophone signals. These fluctuations in response result from the spatiotemporal variation in bed load flux [*Habersack et al.*, 2001, 2008]. In fact, the sensitive (i.e., acoustically relevant) area of a geophone is limited by the size of the steel plate (0.36 m by 0.5 m), whereas the sensitive area of a hydrophone remains unknown. An approach using partial correlation is hereby proposed to determine the magnitude of the monitoring area of a hydrophone.

The sum of specific impulses (IMP$_i$) at a given geophone during each period is denoted SumIMP and is used below. Basic information is contained in the correlation coefficients between measurements of the hydrophone and each individual geophone (Figure 8). Correlation coefficients were high between hydrophone response and those geophones showing significant activity (Figure 8). However, near the banks and where bed load activity was generally weak, correlation coefficients were low. During periods A and B, the correlation profile was slightly asymmetric with a maximum correlation located at 5 and 6 m from the hydrophone, while the maximum recorded geophone activity was observed in the middle of the Drau channel, at 9 m from the hydrophone location. We therefore conclude that during these high flow periods, the hydrophone signals were better represented by the closest geophones rather than by geophones recording the strongest bed load activity. In contrast, during low flow period C, the hydrophone response was better correlated with the geophones located in the middle of the channel, where bed load activity was strongest.

Even though correlation coefficients supply information on the spatial dependence of the hydrophone ($p_{rms,b}$), it is difficult to conclude which parts of the river are "heard" by the hydrophone. When geophone signals showed strong activity, they were, indeed, altogether strongly correlated. This means that if the hydrophone is well correlated to one geophone, it is therefore correlated to all of the geophones during such events.
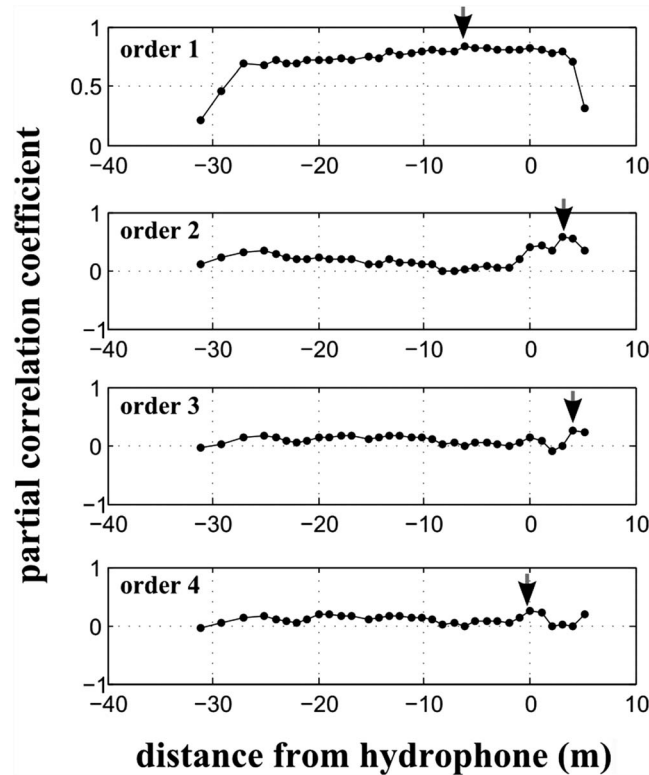
Figure 9. Correlation coefficients and partial correlation coefficients between hydrophone $p_{rms,b}$ value (1–60 kHz) and each particular geophone (SumIMP) during period B. The arrows indicate the maximum correlation observed and, therefore, the geophones added to the explanatory variables. Geophones are represented by their distance to the hydrophone ($X_{h,i}$).

Nevertheless, the entire variance of the acoustic measurements cannot be explained by an individual geophone. Accordingly, we used multiple correlations to explain a maximum of the variance. Particular geophones were selected in turn using a partial correlation-based approach (see supporting information Text S3). An example is presented for period B, in which the four geophones with the best explanatory power are successively selected from correlation analysis (Figure 9). In step one, regression between $p_{rms,b}$ and $SumIMP_i$ identifies the geophone that is best correlated with the hydrophone (Figure 9, first panel). Partial correlations coefficients were then computed for the residuals of this regression to identify the geophone with the second best explanatory power (Figure 9, second panel) and so on until four geophones were selected (Figure 9, third and fourth panel). Further details of the approach are given in the supporting information.

By using one to four geophones, values of multiple correlation coefficients increased from five to seven points during the three periods (Figure 10). After the third iteration (>2 selected geophones) additional information was redundant or irrelevant. As stated earlier, during high flow periods (A and B), hydrophone response was better explained by the closest geophones. Considering the second-order partial correlation coefficient, the second geophone that best explained hydrophone variance was located near the right bank (G#35 located at $X_h = 3.1$ m from the hydrophone for periods A and B, Figures 10a and 10b). We explain this maximum by the fact that this geophone recorded different variations

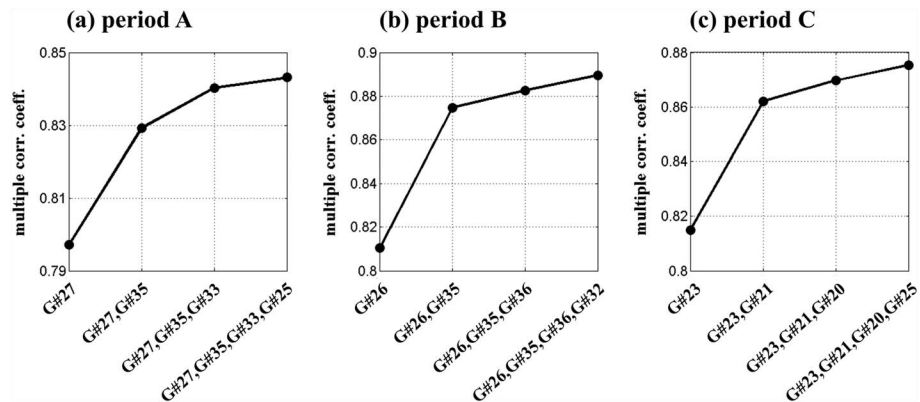**Figure 10.** Multiple correlation coefficients between hydrophone $p_{rms,b}$ (Pa) and SumIMP (imp m^{-1} min^{-1}) of the selected geophones (G#). Abscissas relate to the chosen geophone according to the method described in Figure 9: (a) period A, (b) period B, and (c) period C. Geophones G#1 and G#40 are located near the left and right banks, respectively. The hydrophone is in line with geophone G#32.

from the mean recordings for the entire cross section. In particular, this geophone recorded phases of activity and inactivity, whereas a majority of the geophones were fully active during the floods. As this geophone is relatively close to the hydrophone, it suggests that the hydrophone is partially affected by local bed load transport processes. During period C the hydrophone was better correlated with the geophones located in the middle of the river than with the closest geophones. This may be explained either by the lack of activity of bed load transport near the hydrophone or by the lack of ability of the geophone system to sense low bed load fluxes. As bed load fluxes were weaker during this period, we wonder whether they were sufficiently strong to generate an acceptable signal-to-noise ratio by the geophones located near the hydrophone.

4. Discussion

4.1. The Drau Soundscape

Root-mean-square acoustic pressures ($p_{rms,b}$) recorded in the Drau River during spring and summer periods varied from 3 to 60 Pa (1–60 kHz), which are fairly large; prior studies of riverine environments report values in the range of 0.005 to 30 Pa [*Tonolla et al.*, 2010, 2011; *Wysocki et al.*, 2007; *Bassett et al.*, 2013; *Lorang and Tonolla*, 2014]. The soundscape of the Drau River is, therefore, a powerful acoustic environment. Origins of ambient noise can be attributed to a variety of processes occurring in a river. In particular, flowing water can generate high acoustic pressure in turbulent environments [*Tonolla et al.*, 2009; *Vračar and Mijić*, 2011; *Lorang and Tonolla*, 2014]. Human activities, such as boat traffic or nearby road traffic, are also suspected of generating high acoustic pressure above 1000 Hz [*Vračar and Mijić*, 2011]. In our study, we propose that low-frequency noise (<100 Hz) is generated by turbulence in the absence of bed load transport, while bed load-generated noise is characterized by a continuous field of impulses at high frequencies (>1000 Hz). Turbulent-induced noise contributed to about 5–20% of the total acoustic energy, varying with hydrologic conditions. It exhibited high spectral power but in a limited frequency range (10–100 Hz). The signal was dominated by bed load self-generated noise over a wideband of frequencies (1000–100,000 Hz). The contribution of bed load transport increased faster than turbulence-induced noise with increasing hydrodynamic conditions.

Theoretical and laboratory-based studies have shown that p_{rms} is proportional to Q_s^γ, with γ varying between 0.5 and 1 [*Johnson and Muir*, 1969; *Thorne*, 1985, 1986, 2014]. We find a somewhat lower exponent 0.37 (see equation (15)) that may be explained by the mode of particle transport. If particles move as a traction carpet at our study site, the sound generated from this transport may not be as loud as saltating grains, which likely impact the river bed at higher velocities. In addition, uncertainties related to the total bed load flux estimate have to be considered, as the geophone array has been calibrated for diameters larger than 21 mm.

For the first time in a natural stream, a relationship between acoustic pressure and total bed load flux has been established (Figure 7). Obtaining several weeks of continuous data enabled us to observe high correlation between acoustic pressure (p_{rms}) above 1 kHz and the total bed load activity monitored by a geophone array (Table 1). This result proves that passive acoustic measurements are well suited for monitoring bed load flux in large gravel bed rivers.

4.2. Geophone Versus Hydrophone

Changes in the relationship between hydrophone ($p_{rms,b}$) and geophones ($\overline{IMP}$) at low flow need to be addressed. Although geophone and hydrophone signals are well correlated during high flows, when bed load transport produces high impulse counts (Figure 7, IMP ≥ 1), the relationship breaks down at lower flows with fewer impulses (Figure 7, IMP < 1). Using equations (2) and (3), we calculate from the hydrophone that bed load grain sizes were in the range of 10–40 mm during low flows (depths less than 120 cm, Figure 6). Because geophones have limited ability to detect movement of grains of diameter smaller than 20–30 mm [*Rickenmann et al.*, 2012], we therefore suspect that the loss of impulse count during low flows can be attributed to fine bed load sizes, rather than to cessation of motion. The higher sensitivity of the hydrophone in comparison to the geophones is explained by two factors. The first concerns the range of monitored frequencies. The hydrophone signals recorded acoustic waves as high as 100 kHz, thereby enabling the detection of sound generated by small particles. According to equation (3), a frequency peak of 100 kHz corresponds to a diameter of 1 mm. Geophone signals are sampled at a frequency of 10 kHz and, therefore, provide information up to 5 kHz. Applying equation (3) to the impact plates system, a frequency peak of 5 kHz is equivalent to a diameter of 30 mm. The use of sensors having a larger range of monitored frequencies increases the lower

limit of the impact plate systems as recently demonstrated [*Barrière et al.*, 2015a]. The second argument is linked to the signal processing methods. Impulse counts are widely used to characterize geophone signals and have been shown to be linearly dependent on bed load mass, which has the advantage of filtering noise that is not impulsive (i.e., turbulence-induced noises). However, it is possible that some transport modes (rolling and sliding particles) [*Krein et al.*, 2008; *Tsakiris et al.*, 2014] or numerous impacts of small gravels do not generate detectable impulses but instead produce "colored" noise. For this reason, and as done for the hydrophone signals, the use of signal energy in useful and relevant frequency bands should provide more representative monitoring of bed load transport, particularly for the initiation and cessation of bed load motion.

4.3. Spectra of Acoustic Signals and Grain Size

Spectra of acoustic signals have been shown to vary with flow depth, and this has been interpreted as a change of bed load grain-size distribution with flow depth. Grain size is related to acoustic signals for uniform sediments [*Thorne*, 1985, 1986; *Thorne and Foden*, 1988; *Belleudy et al.*, 2010], but interpreting the acoustic signal of a sediment mixture is more complex and has not yet been undertaken for bed load self-generated noise. Comparison of bed load grain sizes captured by the slot sampler with those predicted from equations (2) and (3) indicates that (1) the frequency of the maximum of PSD (f_{peak}) leads to the estimation of the largest diameters set in motion (D_{90}) and (2) the central frequency leads to the estimation of D_{50} (Figure 6b). The observed discrepancy is attributed to the nonuniform bed load size distribution, whereas the equations were developed for uniform grain size. For geophone devices, the use of central frequency to estimate median diameters has been demonstrated in the recent study of *Barrière et al.* [2015a]. To confirm the findings of *Barrière et al.* [2015a] for passive acoustic monitoring systems, contemporaneous measurements of grain-size distribution are needed. Despite a lack of such data for the contemporaneous monitoring of the hydrophone and geophones in the Drau River, these findings are of considerable interest as our technique is capable of estimating typical bed load diameters using parameters of spectra shape. By using additional parameters of spectra shape (such as statistical moments and the width of the spectrum at half maximum), it may be possible to estimate the bed load grain-size distribution. Indeed, concomitant monitoring of the current hydrophone and the Reid slot sampler at the Drau is planned and may provide the requisite database. Nevertheless, the frequency content of received acoustic signals is affected not merely by bed load grain size but also by propagation effects. Acoustic signals vary according to the medium in which the acoustic waves propagate, that is, the water column. Acoustic waves interact with the river bed, the water surface, and suspended particles. These interactions are often frequency dependent [*Medwin*, 2005]. For the range of frequencies of interest (<100 kHz), knowledge of acoustic propagation is not well documented in rivers, warranting future investigation.

4.4. Listening Distance

A particular property of hydrophone monitoring is its integrative measurement over an area of the river bed. The hydrophone signal is complex, composed of noise sources derived from different locations at varying distances. An advantage of the integrative measurement is that it is not local and provides information on bed load flux over a larger area of the bed. A disadvantage is that the measurement depends on the location of the acoustic sources. For identical bed load fluxes, the received acoustic energy depends on the distance between the hydrophone and bed load impacts. A process of localizing sound sources appears to be necessary for the quantification bed load flux. We observed that the hydrophone was strongly affected by closest or strongest bed load fluxes. High correlations observed for different periods can be interpreted as the maximum distances to which bed load transport had a relevant effect on hydrophone signals. These distances are estimated to be in the range 5–10 m (Figures 8 and 9), varying according to flow depth. To our knowledge, this is the first attempt to characterize the listening distance of a hydrophone in a river.

Masking effects [*Medwin*, 2005] should constrain the ability of a hydrophone to receive acoustic signals from far-field sources. Considering equation (1), a maximum of bed load noise is generated at the location of maximum bed load transport in the channel cross section. Bed load noise generated farther away is less powerful because of weaker bed load fluxes and due to geometric spreading (higher transmission losses with increasing distance of sound sources toward the hydrophone). An acoustic "barrier" should, therefore, exist and be located near the maximum of bed load transport in the channel cross section, masking bed load noise that is generated farther away. Hydrophone signals should be less integrative when located close to the maximum

of bed load transport. This concept of an acoustic barrier can explain the results of the multiple correlations. Geophones selected to explain a maximum of the hydrophone variance were all located in the right part of the channel, between the maximum of observed bed load flux and the right bank. For a straight, planar reach, we suggest placing hydrophones in the left and right halves of the channel (on either side of the high-energy center line, which may be an acoustic barrier) to provide representative measurements of the total bed load discharge.

5. Conclusions

Our analysis shows that hydrophones can be used to passively monitor the occurrence of bed load transport in a large gravel bed river and to determine the size of the material in transport. By dividing acoustic signals into frequency bands, we were able to distinguish turbulence and other ambient noises from bed load transport, which dominates the signal above 1000 Hz. In addition to detecting the occurrence of bed load transport, the wide range of frequencies that were monitored allowed prediction of the size of bed load material in transport. Spectral parameters, combined with equations developed by *Thorne* [1985, 1986, 2014], enabled us to predict two characteristic sizes of bed load material, which approximate the D_{50} and D_{90} sizes measured in a nearby slot sampler. The ability to passively monitor these particular grain sizes is important, as they are widely used in bed load transport formulae. Comparing measurements across flow depths ranging from 70 to 190 cm revealed similar patterns of acoustic signals and consistent information on bed load transport. Root-mean-square acoustic pressures were highly correlated to mean bed load fluxes monitored by a geophone array. Our study is the first attempt to characterize the listening distance of a hydrophone in a natural gravel bed river, and we find that the hydrophone measurements are representative of a fairly large area of the river bed (5–10 m from the hydrophone). These field observations confirm that passive acoustic monitoring may help to better understand bed load dynamics. The passive acoustic method is relatively cheap and easy to deploy, providing integrative, continuous monitoring. In terms of future research, additional knowledge is needed to fully interpret the acoustic signals, particularly in terms of sound source localization and propagation effects, and, as with any surrogate monitoring technology, the calibration issue is a challenge.

Notation

α	Empirical coefficient as defined in equation (6).
A	Empirical coefficient as defined in equation (13).
A'	Empirical coefficient as defined in equation (14).
β	Empirical coefficient as defined in equation (1).
B	Empirical coefficient as defined in equation (13).
B'	Empirical coefficient as defined in equation (14).
D	Particle diameter (m).
D_{10}	Diameter of which 10% of the sediment is finer (m).
D_{50}	Median particle diameter (m).
D_{90}	Diameter of which 90% of the sediment is finer (m).
f_c	Central frequency (Hz).
f_{min}	Lowest frequency used in the PSD integral (Hz).
f_{max}	Highest frequency used in the PSD integral (Hz).
f_{peak}	Frequency corresponding to the maximum of the power spectral density (Hz).
γ	empirical parameter as defined in the equation (1).
h	water depth (m).
l	total width of the river (m).
l_i	representative width of geophone i (m).
k	empirical coefficient as defined in equation (6).
k_b	empirical coefficient as defined in equation (5).
M	bed load transported mass (kg).
IMP	number of detected impulses normalized by the width of the geophone plate and the recording period (imp m^{-1} min^{-1}).

$\overline{\text{IMP}}$	weighted mean of IMP values defined in equation (8) ($\text{imp}\,\text{m}^{-1}\,\text{min}^{-1}$).
IQA	sum of squared amplitudes normalized by the width of the geophone plate and the recording period ($\text{V}^2\,\text{m}^{-1}\,\text{min}^{-1}$).
$\overline{\text{IQA}}$	weighted mean of IQA values defined in equation (9) ($\text{V}^2\,\text{m}^{-1}\,\text{min}^{-1}$).
p_{rms}	root-mean-square acoustic pressure (Pa).
$p_{\text{rms},b}$	root-mean-square acoustic pressure in the 1000–60,000 Hz band (Pa).
$p_{\text{rms},t}$	root-mean-square acoustic pressure in the 10–100 Hz band (Pa).
PSD	power spectral density (Pa^2/Hz).
PSD_{max}	maximum of PSD (Pa^2/Hz).
q_s	specific bed load discharge ($\text{kg}\,\text{m}^{-1}\,\text{min}^{-1}$).
Q_s	bed load discharge (kg/min).
SPD	spectral probability density (Pa^2/Hz).
SumIMP	sum of IMP values during a certain period of time ($\text{imp}\,\text{m}^{-1}\,\text{min}^{-1}$).
X_i	absolute distances along the cross section from left bank (m).
$X_{h,i}$	cross-sectional distance between geophone i and hydrophone (m).

References

Barclay, D. R., and M. J. Buckingham (2013), Depth dependence of wind-driven, broadband ambient noise in the Philippine Sea, *J. Acoust. Soc. Am.*, *133*(1), 62–71.

Barrière, J., A. Krein, A. Oth, and R. Schenkluhn (2015a), An advanced signal processing technique for deriving grain-size information of bedload transport from impact plate vibration measurements, *Earth Surf. Processes Landforms*, *40*(7), 913–924, doi:10.1002/esp.3693.

Barrière, J., A. Oth, R. Hostache, and A. Krein (2015b), Bed load transport monitoring using seismic observations in a low gradient rural gravel-bed stream, *Geophys. Res. Lett.*, *42*, 2294–2301, doi:10.1002/2015GL063630.

Barton, J. S., R. L. Slingerland, S. Pittman, and T. B. Gabrielson (2010), Monitoring coarse bedload transport with passive acoustic instrumentation: A field study, in *Bedload-Surrogate Monitoring Technologies*, U.S. Geol. Surv. Sci. Invest. Rep. 2010–5091, edited by J. R. Gray, J. B. Laronne, and J. D. G. Marr, pp. 38–51, U.S. Geological Surv., Reston, Va.

Bassett, C., J. Thomson, and B. Polagye (2013), Sediment-generated noise and bed stress in a tidal channel, *J. Geophys. Res. Oceans*, *118*, 2249–2265, doi:10.1002/jgrc.20169.

Bedeus, K., and L. Ivicsics (1964), Observation of the noise of bedload, in *General Assembly, Commission on Hydrometry*, pp. 384–390, International Association of Hydrological Sciences, Berkeley, Calif.

Belleudy, P., A. Valette, and B. Graff (2010), Passive hydrophone monitoring of bedload in river beds: First trials of signal spectral analysis, in *Bedload-Surrogate Monitoring Technologies*, U.S. Geol. Surv. Sci. Invest. Rep. 2010–5091, edited by J. R. Gray, J. B. Laronne, and J. D. G. Marr, pp. 67–84, U.S. Geological Surv., Reston, Va.

Burtin, A., R. Cattin, L. Bollinger, J. Vergne, P. Steer, A. Robert, N. Findling, and C. Tiberi (2011), Towards the hydrologic and bed load monitoring from high-frequency seismic noise in a braided river: The "torrent de St Pierre", French Alps, *J. Hydrol.*, *408*(1–2), 43–53, doi:10.1016/j.jhydrol.2011.07.014.

Burtin, A., N. Hovius, B. W. McArdell, J. M. Turowski, and J. Vergne (2014), Seismic constraints on dynamic links between geomorphic processes and routing of sediment in a steep mountain catchment, *Earth Surf. Dyn.*, *2*(1), 21–33, doi:10.5194/esurf-2-21-2014.

Camenen, B., M. Jaballah, T. Geay, P. Belleudy, J. B. Laronne, and J. P. Laskowski (2012), Tentative measurements of bedload transport in an energetic alpine gravel bed river, in *River Flow 2012*, edited by M. Munoz, pp. 379–386, Taylor & Francis Group, London.

Childers, D. (1999), Field comparisons of six pressure-difference bedload samplers in high-energy flow, in *Water Resources Investigations Report 92–4068*, U.S. Geol. Surv., Vancouver, Wash.

Deane, G. B. (1997), Sound generation and air entrainment by breaking waves in the surf zone, *J. Acoust. Soc. Am.*, *102*(5), 2671–2689.

Deane, G. B. (2000), Long time-base observations of surf noise, *J. Acoust. Soc. Am.*, *107*(2), 758–770.

Díaz, J., M. Ruíz, L. Crescentini, A. Amoruso, and J. Gallart (2014), Seismic monitoring of an Alpine mountain river, *J. Geophys. Res. Solid Earth*, *119*, 3276–3289, doi:10.1002/2014JB010955.

Emmett, W. W. (1980), A field calibration of the sediment-trapping characteristics of the Helley-Smith bedload sampler. U.S. Geol. Surv. Prof. Pap. 1139, 44 pp.

Gimbert, F., V. C. Tsai, and M. P. Lamb (2014), A physical model for seismic noise generation by turbulent flow in rivers, *J. Geophys. Res. Earth Surf.*, *119*, 2209–2238, doi:10.1002/2014JF003201.

Gomez, B., R. L. Naff, and D. W. Hubbell (1989), Temporal variations in bedload transport rates associated with the migration of bedforms, *Earth Surf. Processes Landforms*, *14*(2), 135–156.

Gray, J. R., J. B. Laronne, and J. D. G. Marr (2010), Bedload-surrogate monitoring technologies. U.S. Geol. Surv. Sci. Invest. Rep. 2010–5091, pp. 1–37. U.S. Geol. Surv., Reston, Va.

Habersack, H. M., and J. B. Laronne (2002), Evaluation and improvement of bed load discharge formulas based on Helley-Smith sampling in an alpine gravel bed river, *J. Hydraul. Eng.*, *128*, 484–499.

Habersack, H., P. N. Nachtnebel, and J. B. Laronne (2001), The continuous measurement of bedload discharge in a large alpine gravel bed river with a slot sampler, *J. Hydraul. Res.*, *39*, 125–133.

Habersack, H., H. Seitz, and J. B. Laronne (2008), Spatio-temporal variability of bedload transport rate: Analysis and 2D modelling approach, *Geodinamica Acta*, *21*, 67–79.

Habersack, H., H. Seitz, and M. Liedermann (2010), Integrated automatic bedload transport monitoring, in *Bedload-Surrogate Monitoring Technologies*, U.S. Geol. Surv. Sci. Invest. Rep. 2010 – 5091, edited by J. R. Gray, J. B. Laronne, and J. D. G. Marr, pp. 218–235, U.S. Geol. Surv., Reston, Va.

Habersack, H., A. Kreisler, J. Aigner, M. Liedermann, and H. Seitz (2012), Spatio-temporal variability of bedload transport, in *River Flow 2012*, edited by M. Munoz, pp. 423–430, Taylor & Francis Group, London, isbn:978-0-415-62129-8.

Habersack, H., A. Kreisler, R. Rindler, J. Aigner, H. Seitz, M. Liedermann, and J. B. Laronne (2016), Integrated automatic and continuous bedload monitoring in gravel bed rivers, *Geomorphology*, doi:10.1016/j.geomorph.2016.10.020.

Helley, E. J., and W. Smith (1971), Development and calibration of a pressure-difference bedload sampler, U.S. Geol. Surv. Open-File Rep. 73–108, 38 pp.

Hilldale, R. C., W. O. Carpenter, B. Goodwiller, J. P. Chambers, and T. J. Randle (2015), Installation of impact plates to continuously measure bed load: Elwha River, Washington, USA, *J. Hydraul. Eng.*, *141*(3), doi:10.1061/(ASCE)HY.1943-7900.0000975.

Hsu, L., N. J. Finnegan, and E. E. Brodsky (2011), A seismic signature of river bedload transport during storm events, *Geophys. Res. Lett.*, *38*, L13407, doi:10.1029/2011GL047759.

Johnson, P., and T. C. Muir (1969), Acoustic detection of sediment movement, *J. Hydraul. Res.*, *7*(4), 519–540.

Jonys, C. K. (1976), Acoustic measurement of sediment transport, Scientific Series no. 66, Dep. of Fisheries and the Environment, Inland Waters Directorate, CCIW Branch, Burlington, Canada.

Krein, A., H. Klinck, and M. Eiden (2008), Investigating the transport dynamics and the properties of bedload material with a hydro-acoustic measuring system, *Earth Surf. Processes Landforms*, *33*(1), 152–163.

Lauchle, G. C., J. Wang, and M. S. Howe (2002), Flow-induced noise on underwater pressure-vector acoustic sensors, in *OCEANS'02 MTS/IEEE*, vol. 3, pp. 1906–1910, IEEE, doi:10.1109/oceans.2002.1191921.

Loewen, M. R., and W. K. Melville (1991), A model of the sound generated by breaking waves, *J. Acoust. Soc. Am.*, *90*(4), 2075–2080.

Lorang, M. S., and D. Tonolla (2014), Combining active and passive hydroacoustic techniques during flood events for rapid spatial mapping of bedload transport patterns in gravel-bed rivers, *Fundam. Appl. Limnol.*, *184*(3), 231–246, doi:10.1127/1863-9135/2014/0552.

Lugli, M., H. Y. Yan, and M. L. Fine (2003), Acoustic communication in two freshwater gobies: The relationship between ambient noise, hearing thresholds and sound spectrum, *J. Comp. Physiol. A*, *189*(4), 309–320, doi:10.1007/s00359-003-0404-4.

Marineau, M. D., J. T. Minear, and S. A. Wright (2015), Using hydrophones as a surrogate monitoring technique to detect spatial and temporal variations in sediment transport, p. 617–628 in Proc. 10th Federal Interagency Sedimentation Conf., Reno, Nev., 19–23 April.

McEachern, J. F., and G. C. Lauchle (1995), Flow-induced noise on a bluff body, *J. Acoust. Soc. Am.*, *97*(2), 947–953.

Medwin, H. (2005), *Sounds in the Sea: From Ocean Acoustics to Acoustical Oceanography*, Cambridge Univ. Press, New York.

Merchant, N. D., T. R. Barton, P. M. Thompson, E. Pirotta, D. T. Dakin, and J. Dorocicz (2013), Spectral probability density as a tool for ambient noise analysis, *J. Acoust. Soc. Am.*, *133*(4), EL262–EL267.

Mizuyama, T., A. Oda, J. B. Laronne, M. Nonaka, and M. Matsuoka (2010), Laboratory tests of a Japanese pipe hydrophone for continuous monitoring of coarse bedload, in *Bedload-Surrogate Monitoring Technologies, U.S. Geol. Surv. Sci. Invest. Rep. 2010 – 5091*, edited by J. R. Gray, J. B. Laronne, and J. D. G. Marr, pp. 319–335, U.S. Geol. Surv., Reston, Va.

Møen, K. M., J. Bogen, J. F. Zuta, P. K. Ade, and K. Esbensen (2010), Bedload measurement in rivers using passive acoustic sensors, in *Bedload-Surrogate Monitoring Technologies, U.S. Geol. Surv. Sci. Invest. Rep. 2010 – 5091*, edited by J. R. Gray, J. B. Laronne, and J. D. G. Marr, pp. 336–351, U.S. Geol. Surv., Reston, Va.

Moore, S. A., J. Le Coz, D. Hurther, and A. Paquier (2012), On the application of horizontal ADCPs to suspended sediment transport surveys in rivers, *Cont. Shelf Res.*, *46*, 50–63, doi:10.1016/j.csr.2011.10.013.

Mühlhofer, L. (1933), Untersuchungen über die Schwebstoff und Geschiebeführung des Inn nächst Kirchbichl (Tirol) [Suspended sediment and bedload research at the Inn River near Kirchbichl (Tyrol)] [In German.], *Die Wasserwirtschaft*, *1*(6), 23.

Muste, M., S. Baranya, R. Tsubaki, D. Kim, H. Ho, H. Tsai, and D. Law (2016), Acoustic mapping velocimetry, *Water Resour. Res.*, *52*, 4132–4150, doi:10.1002/2015WR018354.

Pijanowski, B. C., A. Farina, S. H. Gage, S. L. Dumyahn, and B. L. Krause (2011), What is soundscape ecology? An introduction and overview of an emerging new science, *Landscape Ecol.*, *26*(9), 1213–1232, doi:10.1007/s10980-011-9600-8.

Reid, I., J. T. Layman, and L. E. Frostick (1980), The continuous measurement of bedload discharge, *J. Hydraul. Res.*, *18*, 243–249.

Rennie, C. D., and M. Church (2010), Mapping spatial distributions and uncertainty of water and sediment flux in a large gravel bed river reach using an acoustic Doppler current profiler, *J. Geophys. Res.*, *115*, F03035, doi:10.1029/2009JF001556.

Rennie, C. D., R. G. Millar, and M. Church (2002), Measurement of bedload velocity using an acoustic Doppler current profiler, *J. Hydraul. Eng.*, *128*, 473–483.

Rickenmann, D., and B. Fritschi (2010), Bedload transport measurements using piezoelectric impact sensors and geophones, in *Bedload-Surrogate Monitoring Technologies, U.S. Geol. Surv. Sci. Invest. Rep. 2010 – 5091*, edited by J. R. Gray, J. B. Laronne, and J. D. G. Marr, pp. 407–423, U.S. Geol. Surv., Reston, Va.

Rickenmann, D., and B. W. McArdell (2007), Continuous measurement of sediment transport in the Erlenbach stream using piezoelectric bedload impact sensors, *Earth Surf. Processes Landforms*, *32*(9), 1362–1378, doi:10.1002/esp.1478.

Rickenmann, D., J. M. Turowski, B. Fritschi, A. Klaiber, and A. Ludwig (2012), Bedload transport measurements at the Erlenbach stream with geophones and automated basket samplers, *Earth Surf. Processes Landforms*, *37*(9), 1000–1011, doi:10.1002/esp.3225.

Rickenmann, D., et al. (2014), Bedload transport measurements with impact plate geophones: Comparison of sensor calibration in different gravel-bed streams, *Earth Surf. Processes Landforms*, *39*(7), 928–942, doi:10.1002/esp.3499.

Rossing, T. D., F. R. Moore, and P. A. Wheeler (2001), *The Science of Sound*, Addison-Wesley, Boston, Mass.

Roth, D. L., N. J. Finnegan, E. E. Brodsky, K. L. Cook, C. P. Stark, and H. W. Wang (2014), Migration of a coarse fluvial sediment pulse detected by hysteresis in bedload generated seismic signals, *Earth Planet. Sci. Lett.*, *404*, 144–153.

Roth, D. L., E. E. Brodsky, N. J. Finnegan, D. Rickenmann, J. M. Turowski, and A. Badoux (2016), Bedload sediment transport inferred from seismic signals near a river, *J. Geophys. Res. Earth Surf.*, *121*, 725–747, doi:10.1002/2015JF003782.

Rouse, H. L. (1994), Measurement of bedload gravel transport—The calibration of a self-generated noise system, *Earth Surf. Processes Landforms*, *19*, 789–800.

Schmandt, B., R. C. Aster, D. Scherler, V. C. Tsai, and K. Karlstrom (2013), Multiple fluvial processes detected by riverside seismic and infrasound monitoring of a controlled flood in the Grand Canyon, *Geophys. Res. Lett.*, *40*, 4858–4863, doi:10.1002/grl.50953.

Strasberg, M. (1979), Nonacoustic noise interference in measurements of infrasonic ambient noise, *J. Acoust. Soc. Am.*, *66*(5), 1487–1493.

Thorne, P. D. (1985), The measurement of acoustic noise generated by moving artificial sediments, *J. Acoust. Soc. Am.*, *78*, 1013–1023.

Thorne, P. D. (1986), Laboratory and marine measurements on the acoustic detection of sediment transport, *J. Acoust. Soc. Am.*, *80*, 899–910.

Thorne, P. D. (1988), Generation of underwater sound by colliding spheres, *J. Acoust. Soc. Am.*, *84*(6), 2144, doi:10.1121/1.397060.

Thorne, P. D. (2014), An overview of underwater sound generated by interparticle collisions and its application to the measurements of coarse sediment bedload transport, *Earth Surf. Dyn.*, *2*(2), 531–543, doi:10.5194/esurf-2-531-2014.

Thorne, P. D., and D. J. Foden (1988), Generation of underwater sound by colliding spheres, *J. Acoust. Soc. Am.*, *84*, 2144–2152.

Thorne, P. D., D. Hurther, and B. D. Moate (2011), Acoustic inversions for measuring boundary layer suspended sediment processes, *J. Acoust. Soc. Am.*, *130*, 1188–1200.

Tonolla, D., M. S. Lorang, K. Heutschi, and K. Tockner (2009), A flume experiment to examine underwater sound generation by flowing water, *Aquat. Sci.*, 71(4), 449–462, doi:10.1007/s00027-009-0111-5.

Tonolla, D., V. Acuña, M. S. Lorang, K. Heutschi, and K. Tockner (2010), A field-based investigation to examine underwater soundscapes of five common river habitats, *Hydrol. Processes*, 24(22), 3146–3156, doi:10.1002/hyp.7730.

Tonolla, D., M. S. Lorang, K. Heutschi, C. C. Gotschalk, and K. Tockner (2011), Characterization of spatial heterogeneity in underwater soundscapes at the river segment scale, *Limnol. Oceanogr.*, 56(6), 2319–2333, doi:10.4319/lo.2011.56.6.2319.

Topping, D. J., S. A. Wright, T. S. Melis, and D. M. Rubin (2007), High-resolution measurements of suspended-sediment concentration and grain size in the Colorado River in Grand Canyon using a multi-frequency acoustic system, *Proceedings of the 10th International Symposium on River Sedimentation*, pp. 330–339, World Association for Sediment and Erosion Research, Moscow.

Tsai, V. C., B. Minchew, M. P. Lamb, and J.-P. Ampuero (2012), A physical model for seismic noise generation from sediment transport in rivers, *Geophys. Res. Lett.*, 39, L02404, doi:10.1029/2011GL050255.

Tsakiris, A. G., A. N. Papanicolaou, and T. J. Lauth (2014), Signature of bedload particle transport mode in the acoustic signal of a geophone, *J. Hydraul. Res.*, 52(2), 185–204, doi:10.1080/00221686.2013.876454.

Turowski, J. M., A. Badoux, and D. Rickenmann (2011), Start and end of bedload transport in gravel-bed streams, *Geophys. Res. Lett.*, 38, L04401, doi:10.1029/2010GL046558.

Vericat, D., M. Church, and R. J. Batalla (2006), Bed load bias: Comparison of measurements obtained using two (76 and 152 mm) Helley-Smith samplers in a gravel bed river, *Water Resour. Res.*, 42, W01402, doi:10.1029/2005WR004025.

Voulgaris, G., M. P. Wilkin, and M. B. Collins (1995), The in situ passive acoustic measurement of shingle movement under waves and currents: Instrument (TOSCA) development and preliminary results, *Cont. Shelf Res.*, 15, 1195–1211.

Vračar, M. S., and M. Mijić (2011), Ambient noise in large rivers (L), *J. Acoust. Soc. Am.*, 130(4), 1787–1791.

Welch, P. D. (1967), The use of fast fourier transform for the estimation of power spectra: A method based on time averaging over short, modified periodograms, *IEEE Trans. Audio Electroacoust.*, AU-15, 70–73.

Wenz, G. M. (1962), Acoustic ambient noise in the ocean: Spectra and sources, *J. Acoust. Soc. Am.*, 34(12), 1936–1956.

Wysocki, L. E., S. Amoser, and F. Ladich (2007), Diversity in ambient noise in European freshwater habitats: Noise levels, spectral profiles, and impact on fishes, *J. Acoust. Soc. Am.*, 121(5), 2559, doi:10.1121/1.2713661.

Wyss, C., D. Rickenmann, B. Fritschi, J. Turowski, V. Weitbrecht, and R. Boes (2016), Measuring bed load transport rates by grain-size fraction using the Swiss plate geophone signal at the Erlenbach, *J. Hydraul. Eng.*, doi:10.1061/(ASCE)HY.1943-7900.0001090,04016003.